POLITECNICO
MILANO 1863

Orbital Mechanic Course

A.Y. 2020/2021

Assignments: Interplanetary & Planetary Explorer Mission

Group 59

Andrea Bersani (880009) - 10523765

Giovanni Chiarolla (964831) - 10801475

Jacopo Fabbri (953163) - 10538161

Matteo Menicaglia (962899) - 10497761

Contents

Nomenclature & Acronyms 3
1 Interplanetary Explorer Mission 4
1.1 Design Procedure 4
1.1.1 Design Constrains 4
1.1.2 Grid Search Optimization 6
1.1.3 Gradient-based Optimization 7
1.1.4 Selection of a Final Solution 7
1.2 Results and Conclusions 8
1.2.1 Heliocentric Trajectories 8
1.2.2 Powered Gravity Assist 9
1.2.3 Total Mission Cost 10
2 Planetary Explorer Mission 11
2.1 Initial Orbit Characterization 11
2.2 Ground Tracks 12
2.3 Orbit Propagation 16
2.4 Filtering of High Frequencies 20
2.5 Comparison with Real Data 20
Bibliography 22

Nomenclature & Acronyms

Nondimensional Quantities

e	Eccentricity	$[-]$
C_D	Drag coefficient	$[-]$
J_2	Second zonal harmonic	$[-]$

Physical Quantities

θ	True Anomaly	$[deg]$
λ	Longitude	$[deg]$
μ	Gravitational Parameter	$[km^3/s^2]$
ϕ	Latitude	$[deg]$
ω	Argument of Periapsis	$[deg]$
$\omega_\oplus$	Earth's rotation rate	$[rad/s]$
Ω	RAAN	$[deg]$
a	Semi-Major Axis	$[km]$
A	Area	$[m^2]$
i	Inclination	$[deg]$
m	Mass	$[km]$
M	Mean Anomaly	$[deg]$
r	Relative Distance	$[km]$
R	Radius	$[km]$
T	Orbital Period	$[s]$
V	Heliocentric Velocity	$[km/s]$
v	Relative Velocity	$[km]$
$\underline{a}$	Acceleration	$[km/s^2]$
A_{cross}	Reference area	$[m^2]$
$\underline{v}_{rel}$	Air-relative speed	$[km/s]$
ρ	Atmospheric density	$[kg/m^3]$

Subscripts & Superscripts

dep	Departure
arr	Arrival
tot	Total
$\oplus$	Earth

Acronyms

DoF	Degree of Freedom
AU	Astronomical Unit
PGA	Powered Gravity Assist
RAAN	Right Ascension of the Ascending Node
SOI	Sphere of Influence
ODE	Ordinary Differential Equation
S/C	Spacecraft
O(n)	Order of Magnitude

Reference frames

$[\hat{\imath}, \hat{\jmath}, \hat{k}]$	Earth centered
$[\hat{r}, \hat{s}, \hat{w}]$	Radial-transversal-out of plane

1 Interplanetary Explorer Mission

The PoliMi Space Agency is carrying out a feasibility study for a potential Interplanetary Explorer Mission visiting three planets in the Solar System.

The aim of this first chapter is to perform a preliminary mission analysis, which consists in the study of the possible transfer options from the departure planet (Mars) to the arrival planet (Mercury), with a powered gravity assist flyby at Venus.

The choice of the best interplanetary trajectory will be based on the mission cost (measured through the total Δv).

The launch provider has set that earliest departure and latest arrival date to be respectively 2031/6/1 and 2071/6/1.

1.1 Design Procedure

The design of the interplanetary trajectory will be based on the patched conics method, resulting in two Lambert's arcs (Mars–Venus, Venus–Mercury) connected by a fly-by around Venus.

Planetary departure and insertion will not be considered for this preliminary design: which means that initial heliocentric orbit is equal to that of the departure planet, and final heliocentric orbit is equal to that of the arrival planet.

The design process can be considered as an optimization problem that will be carried out throughout two different strategies:

- A grid search over the 3 **DoFs** (time at departure, fly-by and arrival)
- A gradient-based optimizer (***fmincon***)

Some preliminary analysis has been conducted and additional constraints added to reach a more precise result and reduce the computational time.

1.1.1 Design Constrains

One of the most important aspects of the design process is the proper selection of the time windows.

Considering that the time constrains given by the launcher provider consist in a very wide range of time (40 years) we need to define smaller time windows in order to enhance the precision and reduce the time of computation.

Thus, we produced the porkchop plots for each transfer arc, to determine the best departure and arrival time for each transfer.

The table below shows the results of this analysis.

Table 1 Results of the preliminary analysis on each transfer arcs

	Mars-Venus arc	Venus-Mercury arc
Departure time	2045/8/18 16:16:5	2032/9/1 10:42:19
Arrival time	2046/4/27 17:33:51	2032/11/4 8:56:50
Δv (km/s)	10.4656	13.1884

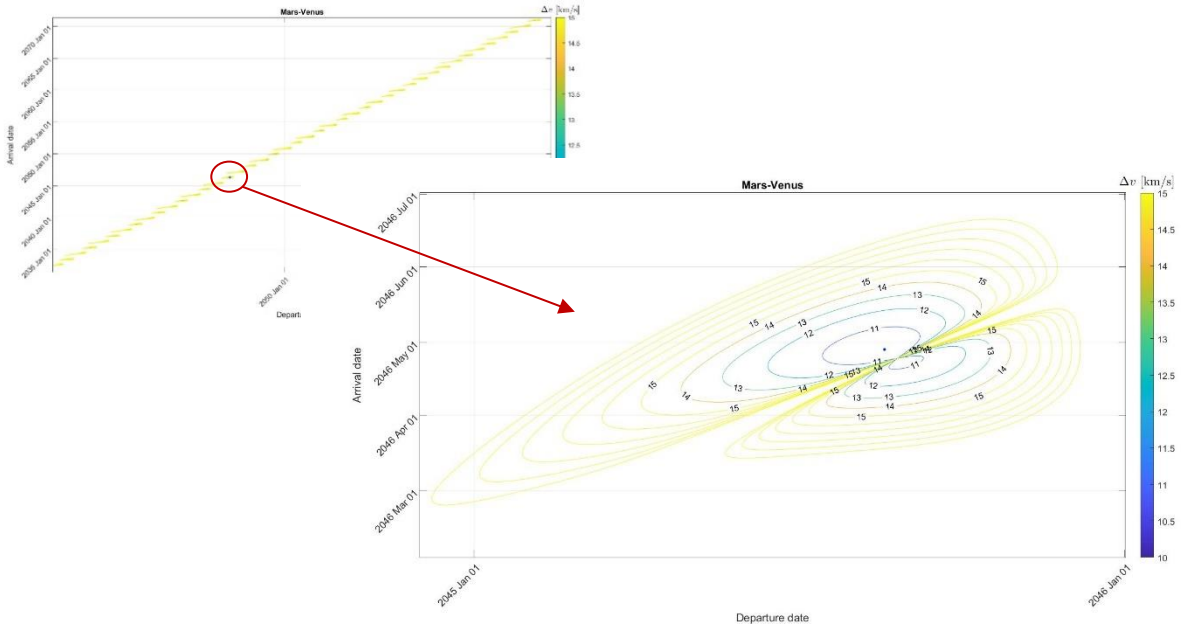

Figure 1 Porkchop plots for the Mars-Venus arc

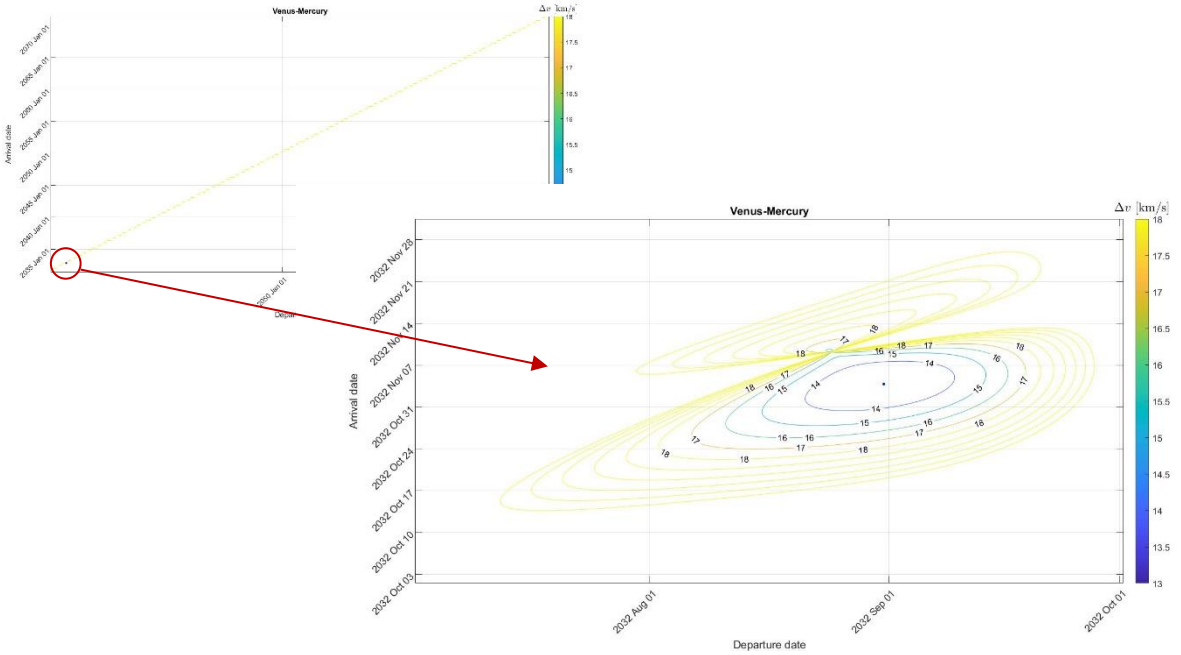

Figure 2 Porkchop plots for the Venus-Mercury arc

Considered that our mission is within the inner planets of the solar system and that therefore the synodic periods are relatively small with reference to a 40 years' time span (Mars-Venus: 335 days, Venus-Mercury: 145 days) the repetition frequency for the possible transfer is high.

Therefore, we decided for the following time windows set at the beginning of the total time span given to us by the launch provider in order to optimize the second transfer arc which has the higher cost.

Table 2 Selected time windows

	Min departure time	**Max arrival time**
Departure	2031/6/1 0:0:0	2037/6/1 0:0:0
Fly-by	2032/2/1 0:0:0	2038/5/1 0:0:0
Arrival	2032/4/1 0:0:0	2038/6/1 0:0:0

An additional constrain has been added concerning the minimum altitude for the fly-by of Venus. We set a minimum altitude for the closest approach of **350 km** to avoid entering Venus atmosphere.

1.1.2 Grid Search Optimization

The grid search optimization consists in the use of three loop cycles in order to create a 3D array containing the Δv for all the possible trajectories that could be performed within the defined time windows.

The operation of the algorithm can be summarized as follows.

Grid search optimization algorithm

```
for all possible departure time
  for all possible fly-by time
    for all possible arrival time
      compute the transfer time for the first arc (Mars-Venus)
      compute the transfer time for the second arc (Venus-mercury)
        if the transfer time is non negative
          compute first Lambert's arc
          compute second Lambert's arc
          compute the PGA given the incoming and outcoming heliocentric velocities
          compute total cost and fill the corresponding entry in the 3D array
        end if
      end for
    end for
```

end for

Search for the smallest value of Δv_{tot} which respect the constrains

The precision of this method is directly correlated to the number in which the time windows are divided: as the number of steps increase the precision of the method is enhanced.

However, increasing the number of steps also means increasing the computational time, therefore it's important to find the best tradeoff between the cost in time and the precision.

We found that divide each time windows in 100 steps offered the best achievable compromise between precision and a reasonable time of computation.

1.1.3 Gradient-based Optimization

Using the grid search optimization algorithm, it was possible to find the minimum Δv needed by the transfer.

It is also possible to perform a further optimization using a gradient-based algorithm. In this assignment it is chosen the MATLAB ***fmincon*** function with a step tolerance of 1e-12 and an optimality tolerance of 1e-12.

Since a gradient based algorithm needs an initial condition, the initial conditions chosen in this project are the solution of the grid search optimization algorithm.

The MATLAB function ***fmincon*** is based on a constrained gradient optimization algorithm so, it is necessary to add constrains. The constrains added are the minimum radius of perigee of the hyperbolic orbit during the fly-by, the departure planet, the fly-by planet and the arrival planet.

1.1.4 Selection of a Final Solution

Through the grid search optimization algorithm, we reach the following solution.

Table 3 Results of the first optimization

Departure	Fly-by	Arrival	Δv (km/s)
2035/11/25 11:09:05	2036/07/01 19:52:44	2037/01/16 13:19:60	20.2490

Then a second optimization has been operated through a gradient-based optimization function to reach the final solution.

Table 4 Final solution (result of the second optimization)

Departure	Fly-by	Arrival	Δv (km/s)
2035/11/25 5:16:29	2036/07/01 20:15:15	2037/01/20 08:43:33	19.4452

As we can see the final solution is a little different from the best transfer option for the second Lambert's arc that we saw with the porkchop plot. This occur because the optimization of a single trajectory may

result in a poor solution for the other one, and also because we need to consider the additional constrain for the fly-by.

This means that this final solution is a tradeoff between the best transfer option for each arc and the PGA constrains.

1.2 Results and Conclusions

1.2.1 Heliocentric Trajectories

The two Lambert's arcs that, compose the selected heliocentric trajectory for the mission, can be characterized by the following Keplerian elements.

Table 5 Characteristics of the heliocentric transfer arcs

	Departure	**Arrival**	a [km]	e [-]	i [deg]	Ω [deg]	ω [deg]	$[\theta_{dep}, \theta_{arr}]$ [deg]
Mars-Venus	2035/11/25	2036/07/01	0.9856	0.4640	2.45	46.34	172.52	[176.92, 82.30]
Venus-Mercury	2036/07/01	2037/01/20	0.7484	0.4353	2.96	68.02	120.60	[112.55, 27.18]

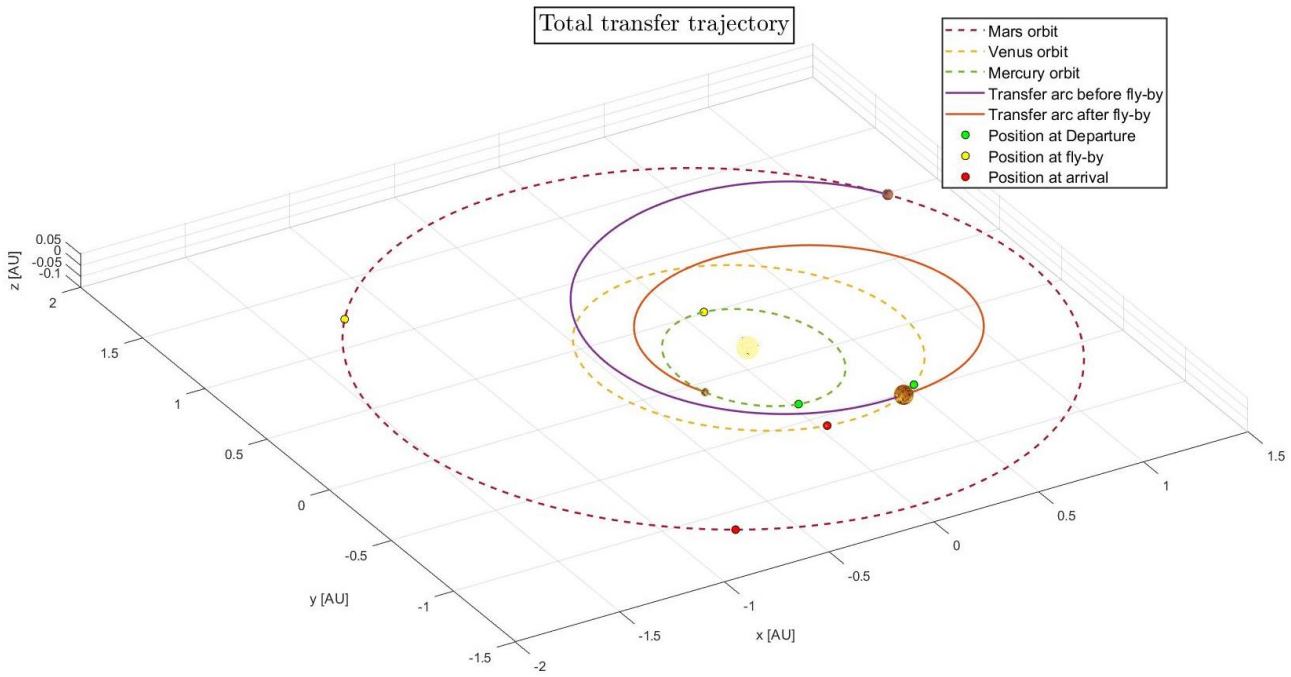

Figure 3 Heliocentric trajectories and position of the planets at departure, fly-by and arrival

1.2.2 Powered Gravity Assist

Knowing the incoming and outcoming heliocentric velocity from the computation of the Lambert's arcs, it was possible to fully characterize the fly-by hyperbola. Since $\underline{v}_\infty^-$ and $\underline{v}_\infty^+$ are different in modulus the fly-by is required to be powered and a $\boldsymbol{\Delta v_{PGA}} = \mathbf{0.0000023}\ \boldsymbol{km/s}$ is applied at the common perigee of the incoming and outcoming hyperbolic arcs.

The characteristic of the fly-by for the final solution are shown in the following table.

Table 6 Characteristic of the incoming and outcoming hyperbolic arcs for the PGA

$\boldsymbol{r_p}$ [km]	$\boldsymbol{h_p}$ [km]	$\boldsymbol{e^-}$ [-]	$\boldsymbol{e^+}$ [-]	$\boldsymbol{v_\infty^-}$ [km/s]	$\boldsymbol{v_\infty^+}$ [km/s]	$\boldsymbol{\Delta v}$ [km/s]	$\boldsymbol{\Delta t_{SOI}}$ [s]
8.6360e+03	2584.18	7.479808	7.479810	15.612500	15.612503	4.1746	2584.18

The duration of the fly-by (considering a finite SOI) has been computed through the hyperbolic time law, considering the intersection points between the two hyperbolic arcs and a sphere with radius

$$\boldsymbol{r_{SOI}} = \mathbf{2.7899e+05}\ \boldsymbol{km}$$

It is possible to highlight that decrease in heliocentric velocity $\boldsymbol{\Delta v}$, achieved after the fly-by, mainly interest the $\boldsymbol{V_x}$ and $\boldsymbol{V_y}$ components.

$$\underline{\boldsymbol{V}}^- = \begin{Bmatrix} 38.8266 \\ 5.2979 \\ -1.0457 \end{Bmatrix} km/s \qquad \underline{\boldsymbol{V}}^+ = \begin{Bmatrix} 35.1778 \\ 3.3526 \\ -1.6199 \end{Bmatrix} km/s$$

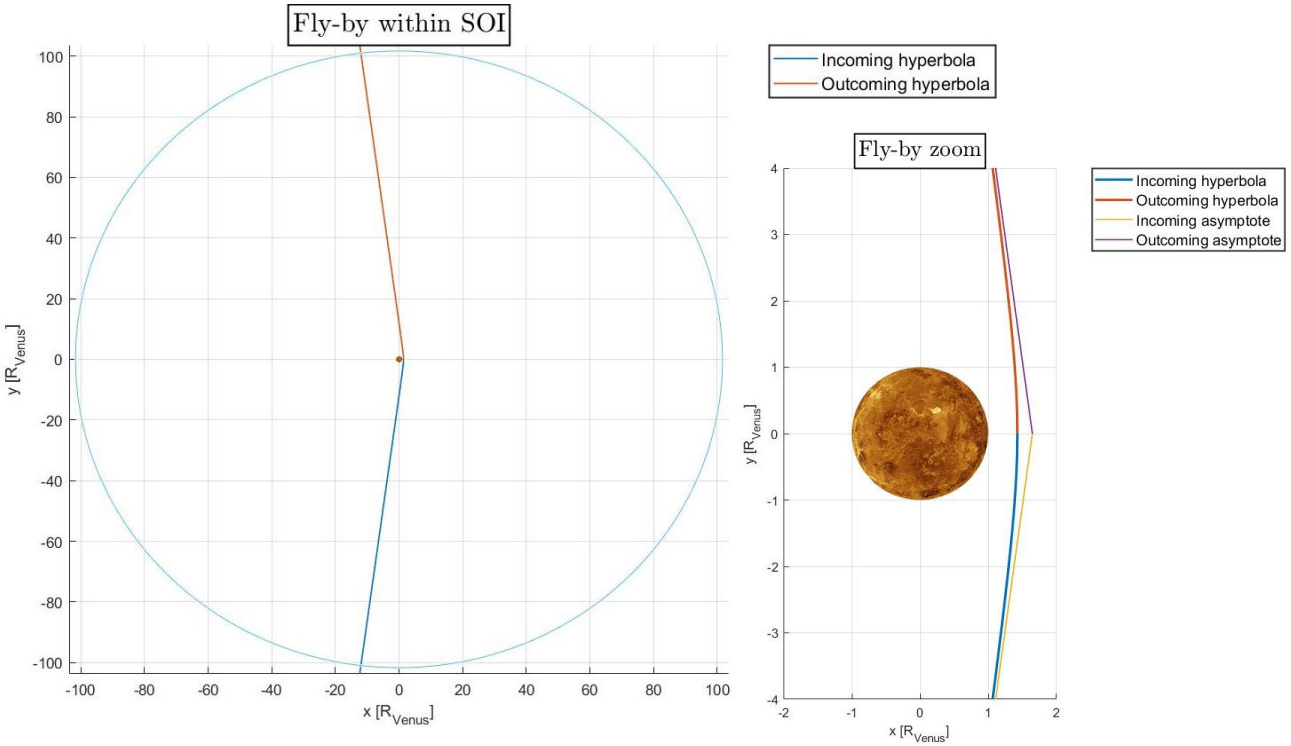

Figure 4 Power gravity assist at Venus

1.2.3 Total Mission Cost

The cost of the mission is shown in detail in the following table.

Table 7 Mission cost

	Δv_{dep}	Δv_{PGA}	Δv_{arr}	Δv_{tot}
Cost of the maneuver [km/s]	7.3104	0.000023	12.1348	19.4452

It is clear that the Δv associated with the power gravity assist is minimal with respect to those associated with the departure and arrival maneuver, and that as anticipated the cost of the arrival maneuver is higher than that of the departure one.

In order to validate our solution we tried to see if it was possible to find a better solution setting our time windows to optimize the first transfer arc. As expected we found a very close solution, due to the high repetition frequency for possible transfer, but with a slightly higher cost. In this way we were able to asset that our solution was the optimal one, also because allows us to start the mission as soon as possible.

2 Planetary Explorer Mission

The PoliMi Space Agency wants to launch a Planetary Explorer Mission, to perform Earth observation.
This part of the report aims at studying the effect of orbit perturbations, in particular, **J2** and **Drag**.
The analysis will also dwell on ground track estimation and implementation & comparison of different propagation methods.

2.1 Initial Orbit Characterization

The initial Earth-centered orbit is characterized by the following orbital elements:

Table 8 Keplerian elements of the initial orbit

a [km]	e [-]	i [deg]	Ω [deg]	ω [deg]	θ [deg]
11111	0.3939	44.0523	60	30	60

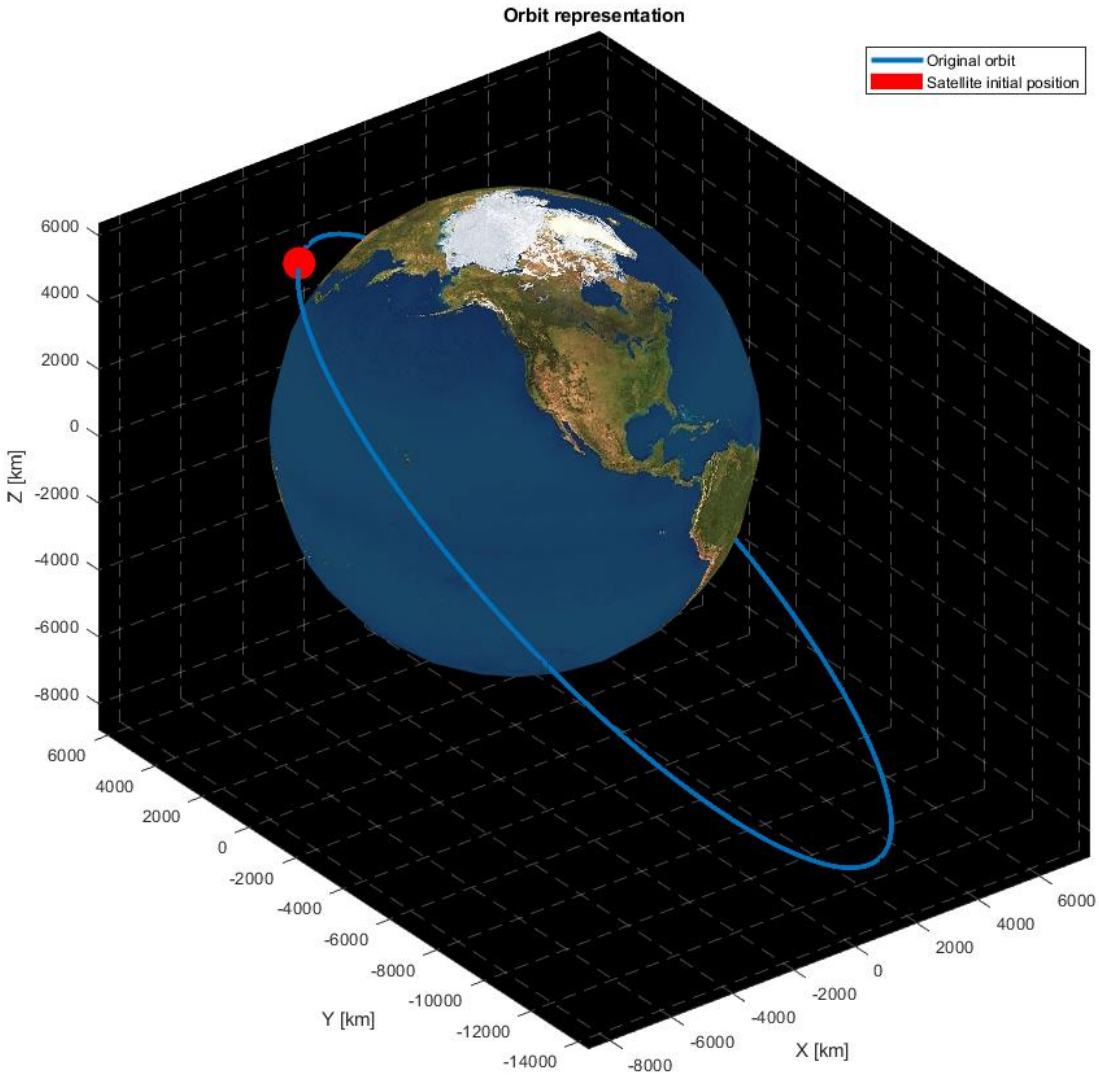

Figure 5 Initial orbit representation

2.2 Ground Tracks

Here is shown the effect of the J2 perturbation on the S/C orbit, with respect to the position of it on the Earth's surface.

Moreover, we consider the difference on the position due to the Earth's rotation, which is avoidable using a semi-major axis which make true the equation between Earth's period $\mathbf{T}_{\oplus}$ and numbers of rotation $\mathbf{m}$, and S/C period $\mathbf{T}$ and numbers of revolutions $\mathbf{k}$:

$$\frac{T}{T_{\oplus}} = \frac{m}{k}$$

a) First, we plotted the ground track over 1 orbit, 1 day, and 10 days, for unperturbed 2BP and for the 2BP perturbed by $J2$:

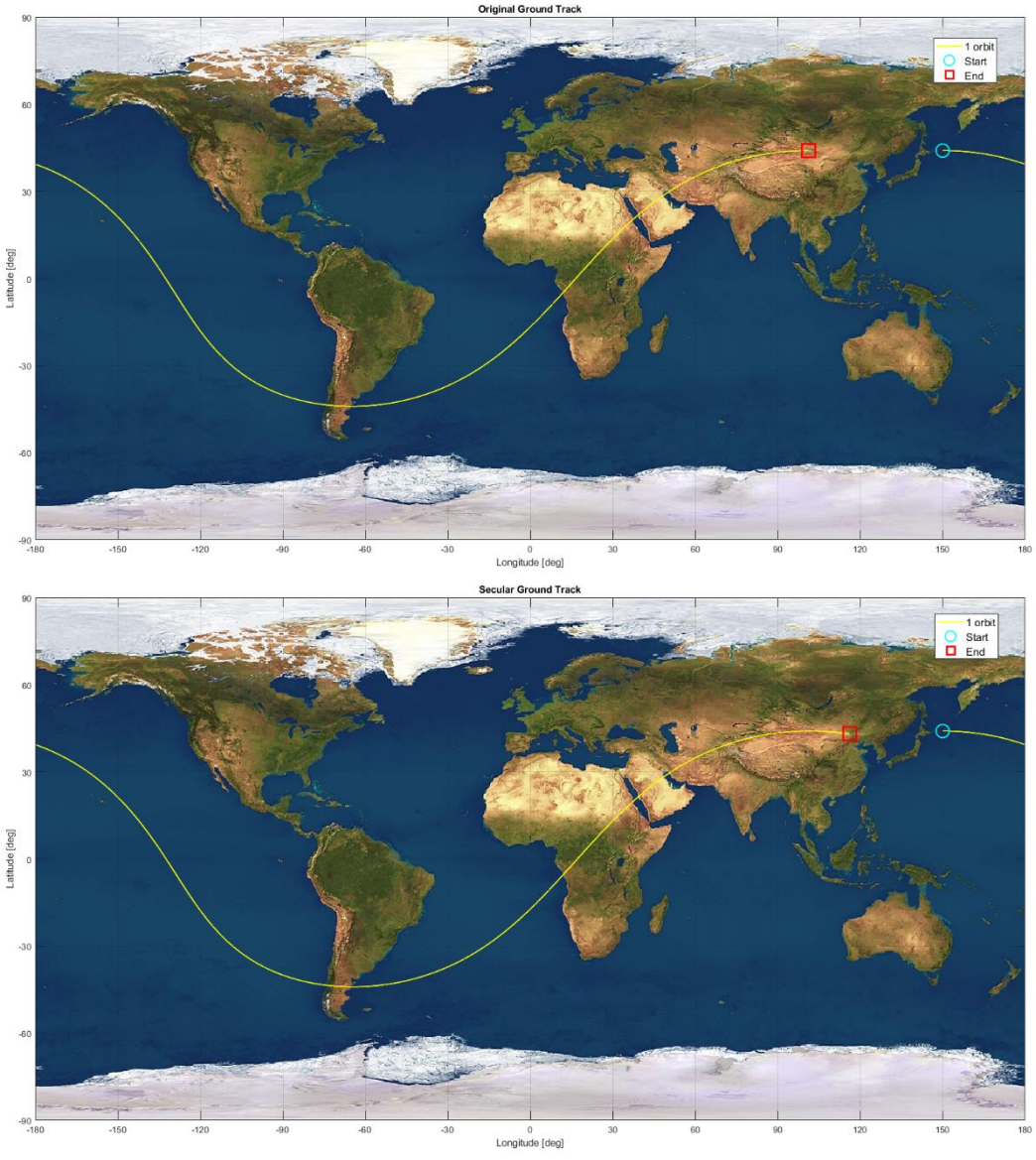

Figure 6 Original Ground Track (Up) and Secular Ground Track (Down) for 1 orbit

As we can see, there is a little difference on the ground track, due to the J2 perturbation.

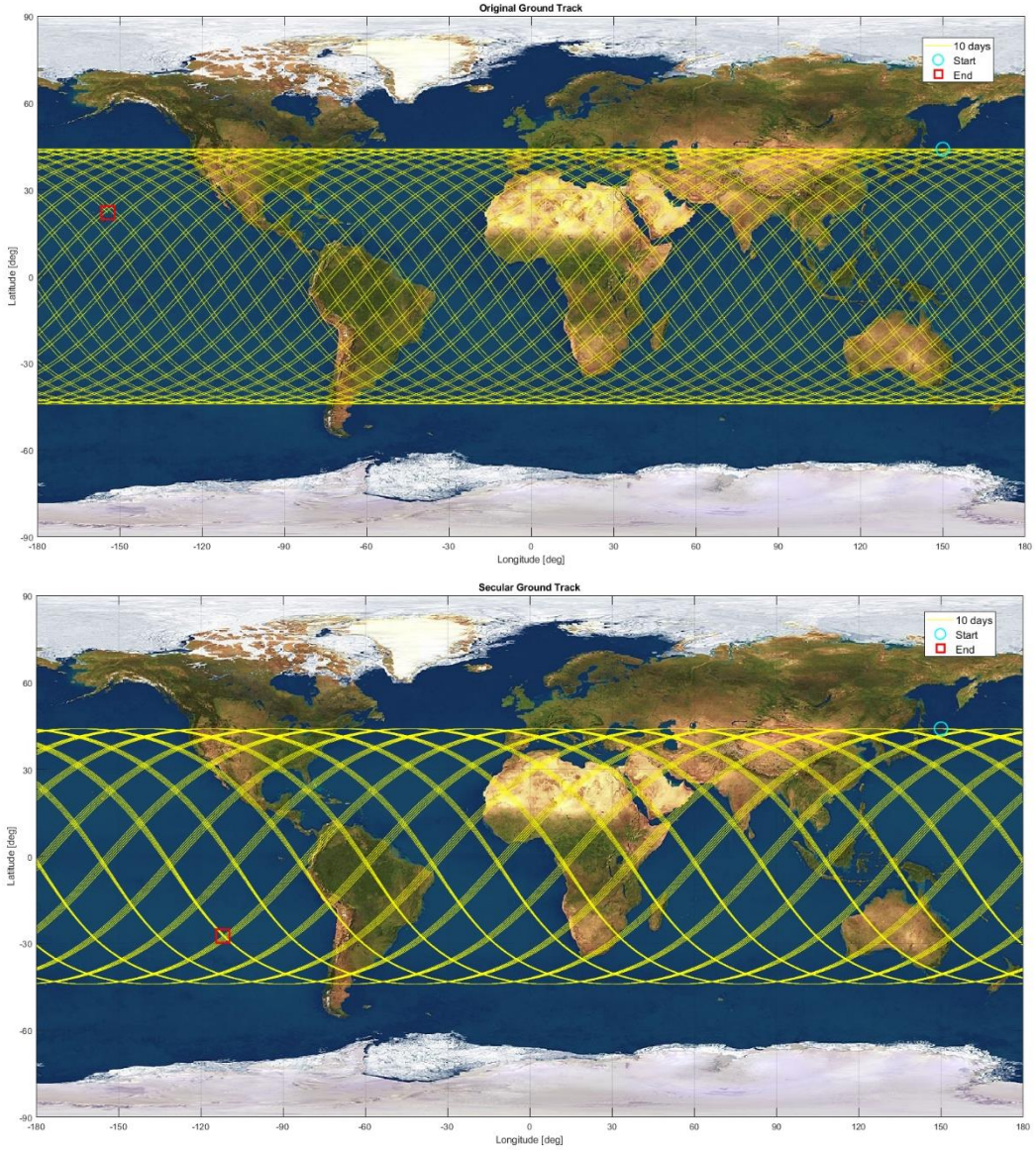

Figure 7 Original Ground Track (Up) and Secular Ground Track (Down) for 10 Days

During 10 days, the difference is quite more considerable.

b) Last, we modified the semimajor axis to obtain a repeating ground track, for the unperturbed case (rotation of Earth) and with secular J_2.
In our case we had as data: **k = 15** and **m = 2**

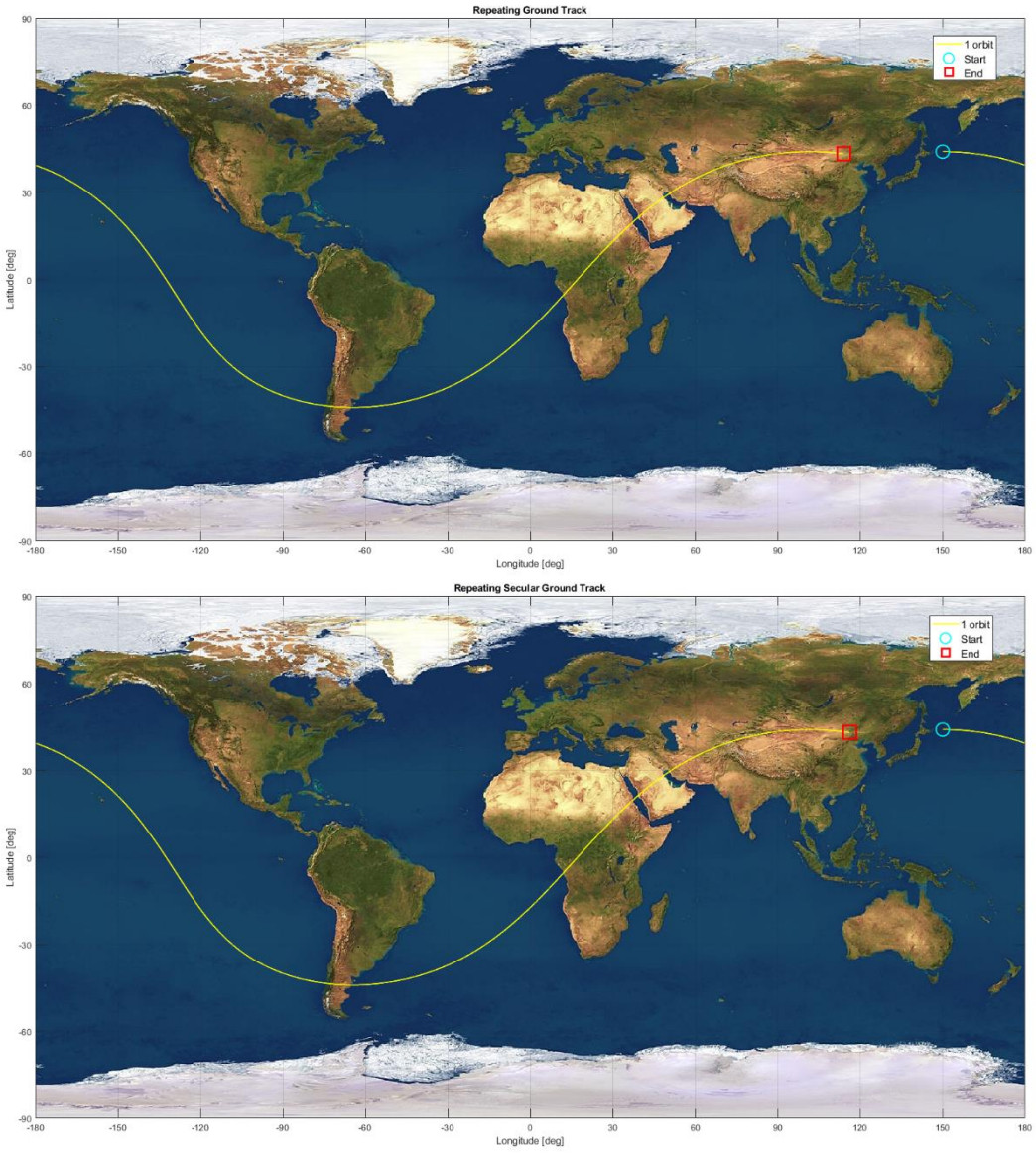

Figure 8 repeating Ground Track (Up) and Repeating Secular Ground Track (Down) for 1 orbit

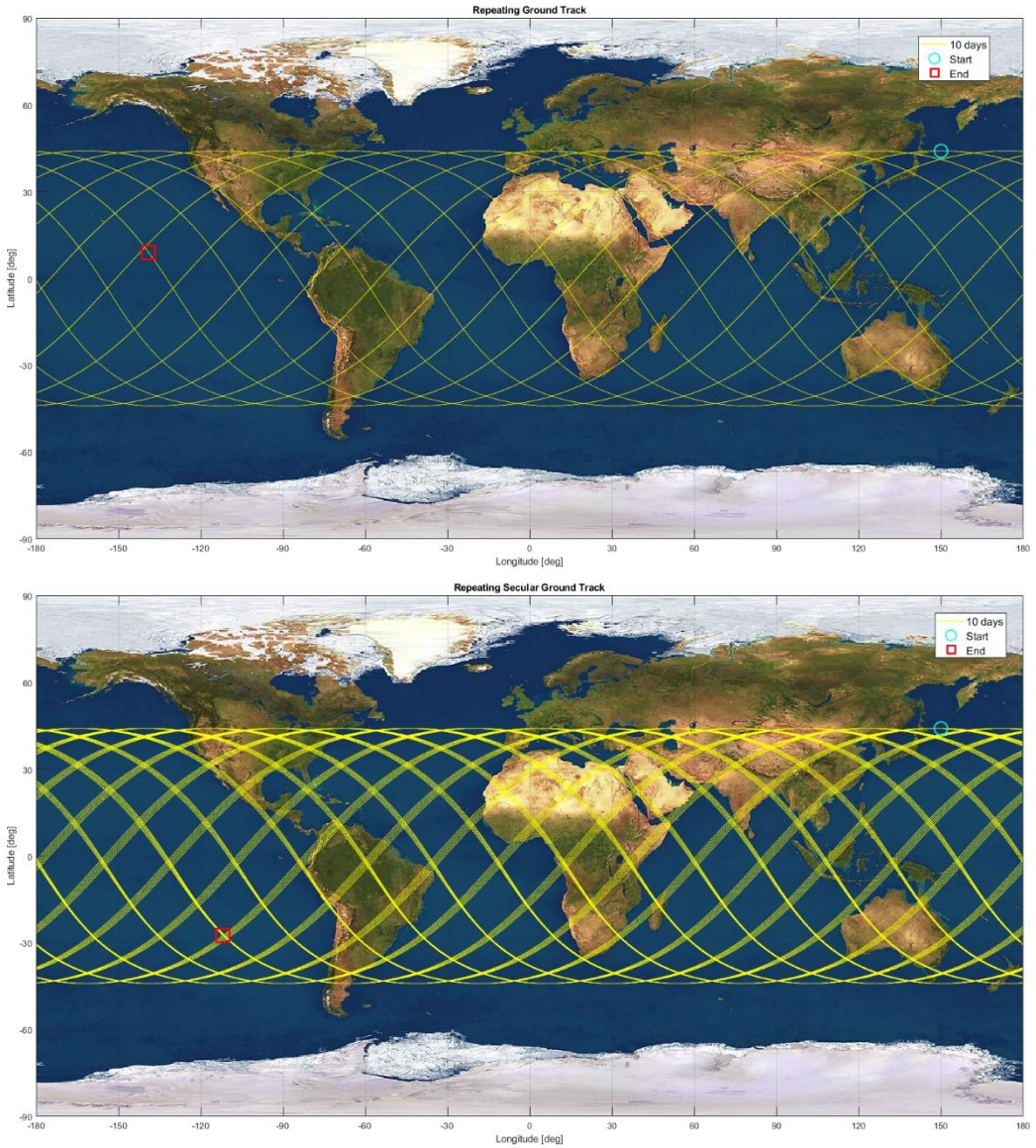

Figure 9 Repeating Ground Track (Up) and Repeating Secular Ground Track (Down) for 10 days

On the 10 days case, the ground track is clearly repeated after 15 S/C revolutions, as we expected from the theory.
The variation due to J_2 is still remarkable, even if less evident than the unperturbed original case: in fact, we can see, from the numerical results, that repeating semi-major axis and secular one, are very close to each other:

Table 9 Semi-major axis for the repeating and secular ground track

$\boldsymbol{a_{rep}}$ $[km]$	$\boldsymbol{a_{sec}}$ $[km]$
11004.997	10980.560

2.3 Orbit Propagation

Orbit propagation will be achieved using two different sets of differential equations, listed below, that will include both the second zonal harmonic perturbation and the aerodynamic drag perturbation. The sets of ODEs that will be solved numerically are:

a) Cartesian coordinates.

$$\ddot{\underline{r}} = -\frac{\mu}{r^3}\underline{r} + \underline{a}_p^{CAR}$$

b) Keplerian elements through Gauss' planetary equations, in a Radial, Transversal, Out of Plane reference frame.

$$\underline{a}_p^{rsw} = [\hat{r} \quad \hat{s} \quad \hat{w}]^T \underline{a}_p^{CAR}$$

$$\begin{Bmatrix} \dot{a} \\ \dot{e} \\ \dot{i} \\ \dot{\Omega} \\ \dot{\omega} \\ \dot{\theta} \end{Bmatrix} = \underline{f}(a, e, i, \Omega, \omega, \theta, \underline{a}_p^{rsw})$$

Then, the time history of positions and velocities of the satellite will be converted in Keplerian elements (through *car2kep.m*) and comparisons can be drawn.
The ODE solver is then used for one thousand periods of the orbit itself, to have a better understanding of the effects of atmospheric drag, which would be too little in magnitude to actually show in a plot for the orbital elements through a shorter amount of time.
The Keplerian elements time evolution is shown below, representing time as periods of the orbit. We obtain, as expected:

1. Secular variations for both Ω and ω due to the second zonal harmonic effect.
2. The semi-major axis and the eccentricity both decrease over a longer time period, as an effect of aerodynamic drag.
3. Solutions oscillating at high frequency (shorter amounts of time).

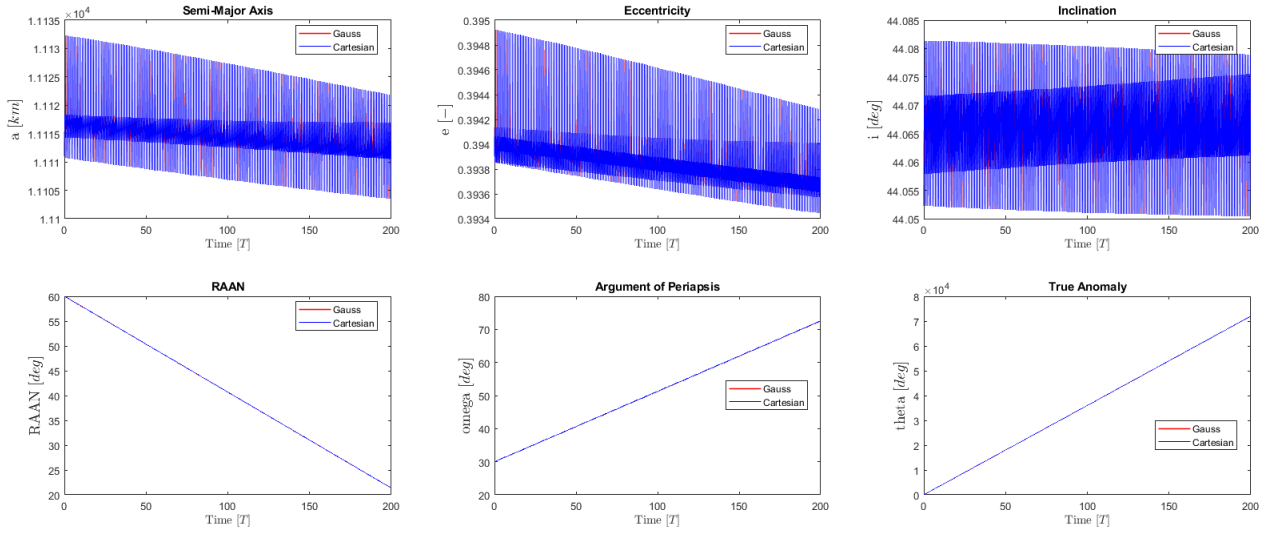

Figure 10 Gauss (Red) and Cartesian (Blue & thinner to show Gauss) equations Keplerian parameters time evolution over 200 orbits

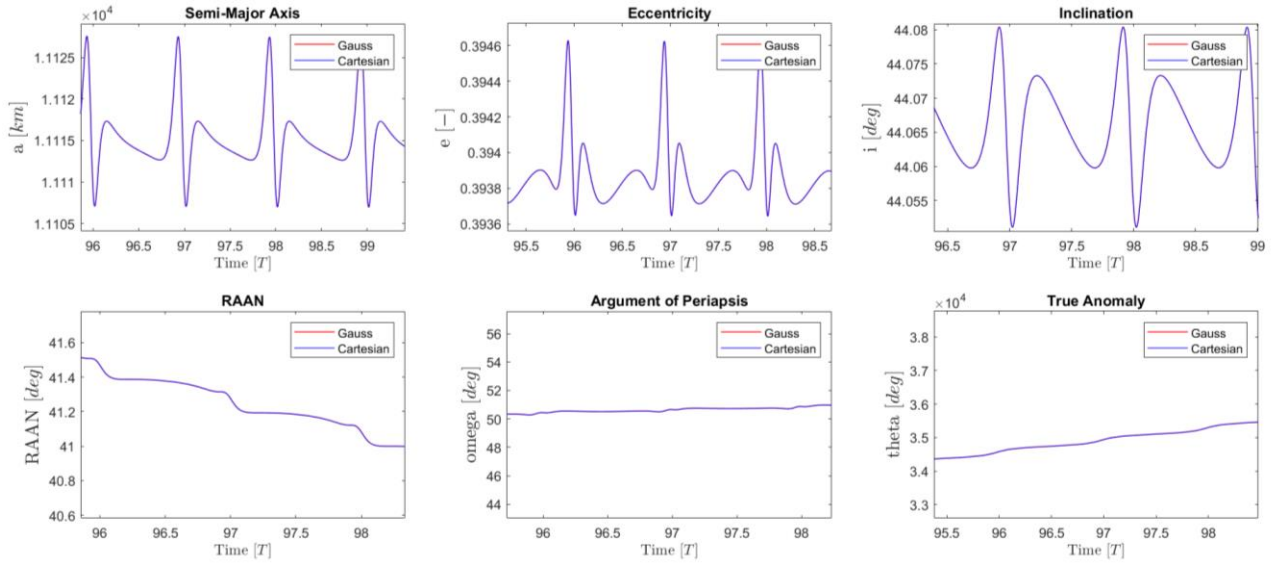

Figure 11 Details of the Keplerian elements shown in Figure 12

Both propagation methods are based off using numerical ODE solvers to different sets of equations.
It can be shown that, by using the same tolerance for either method (Relative Tolerance =10^{-13}, Absolute Tolerance = 10^{-11}) the two don't differ in terms of accuracy, as the infinity norm of the relative error of each parameter, normalized with the initial value for it, and the plot of these relative errors are close to the round-off error.

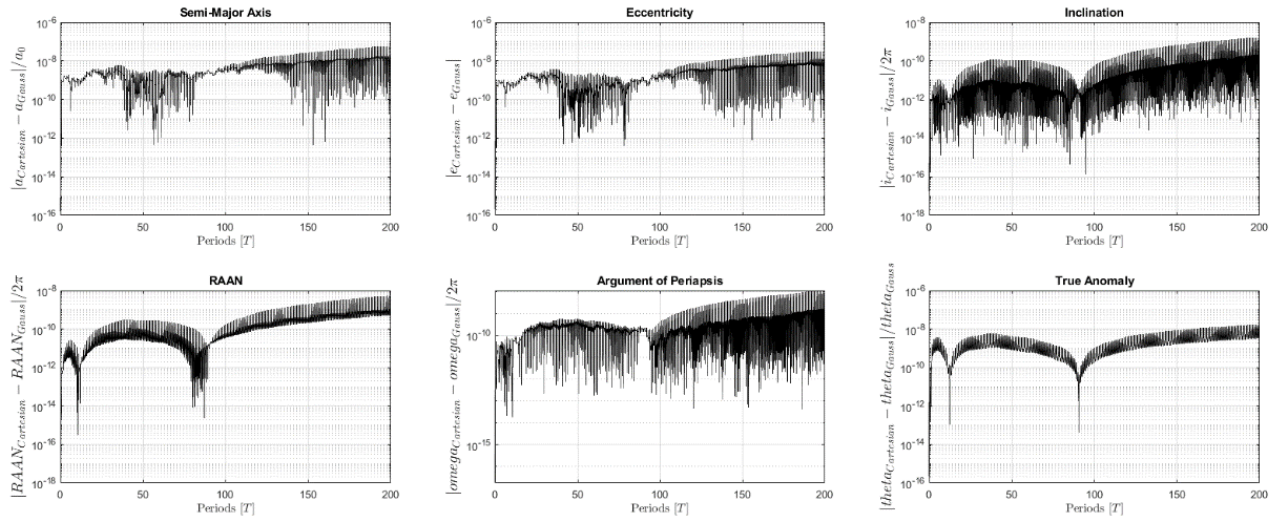

Figure 12 Errors on Keplerian parameters obtained through the two sets of equations over 200 orbits

Table 10 Errors in norm infinite for each Keplerian element for the two sets of equations

	a	e	i	Ω	ω	θ
err_∞ [-]	1.692e-08	1.092e-08	5.311e-10	1.575e-09	2.940e-09	6.394e-06

Another interesting approach to precise for either method is computational time.
The CPU time for either method is evaluated by repeating simulations with increasing sized time vectors, input for the ODE solver, over a fixed span of 100 orbits. Then, results are plotted for both sets of equations for comparison. Data can be approximated well through the best-fit lines for both, although the slopes of the lines are of the order of 10^{-6}.

From an algorithm point of view, they are the same in terms of computational time, being **O(n)**.
It's important to note, however, that through Gauss equations the obtained results are directly Keplerian elements, while for Cartesian coordinates a *for* cycle (heavy in terms of CPU time) to convert results from $\underline{\boldsymbol{r}}$,$\underline{\boldsymbol{v}}$ to Keplerian elements is needed, thus the former are considered better.

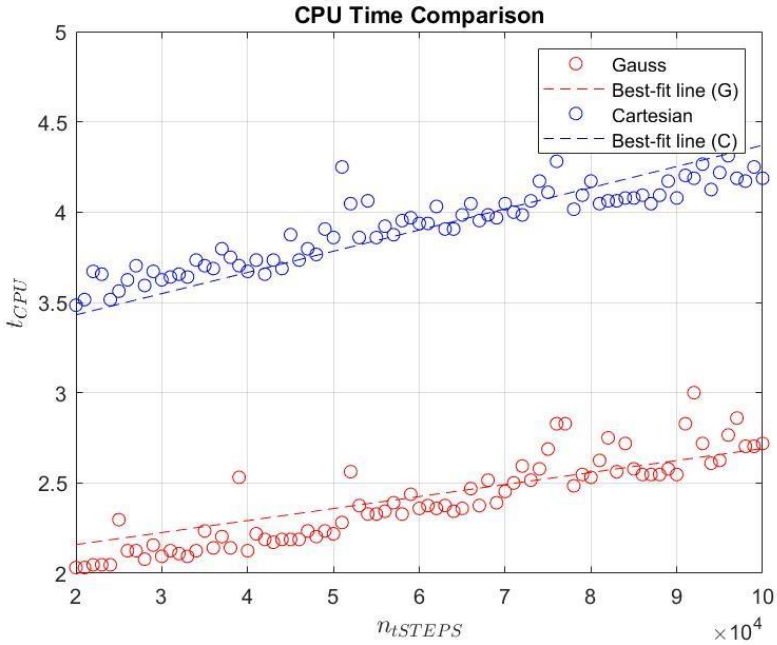

Figure 13 Evolution of time cost with respect to the number of time steps over 100 orbits

Having discussed both accuracy and CPU time to obtain the evolution of the orbit over time, a graphical representation through Gauss equations is obtained. *Figure 14* shows the evolution over 200 orbits, which equals to about a month. The effects of J2 are clear: both RAAN and the apse line direction are visibly changed even in such a little period.

$$\underline{\boldsymbol{a}}_{J_2} = \frac{3}{2}\frac{J_2 \mu R_\oplus^2}{r^5}\left[\left(5\frac{z^2}{r^2}-1\right)x\hat{\imath} + \left(5\frac{z^2}{r^2}-1\right)y\hat{\jmath} + \left(5\frac{z^2}{r^2}-1\right)z\hat{k}\right]$$

Aerodynamic drag's magnitude as a perturbing acceleration is much lower, so it can't be shown in *Figure 15*.

To have a graphical representation for drag effects, **J2** is then ignored, and the time window over which the evolution is simulated is over 100000 periods, resulting in roughly 35 years, confirming that aerodynamic drag has much less short-period impact on orbit than the second zonal harmonic. It's still worth noting, however, that both semi-major axis and eccentricity decrease accordingly to theory about aerodynamic drag, and while the height of perigee is about the same, the height of apogee decreases over the years.

$$\underline{\boldsymbol{a}}_{Drag} = -\frac{1}{2}\frac{A_{cross} C_D}{m}\rho(h,t) v_{rel}{}^2 \frac{\underline{v}_{rel}}{\|\underline{v}_{rel}\|}$$

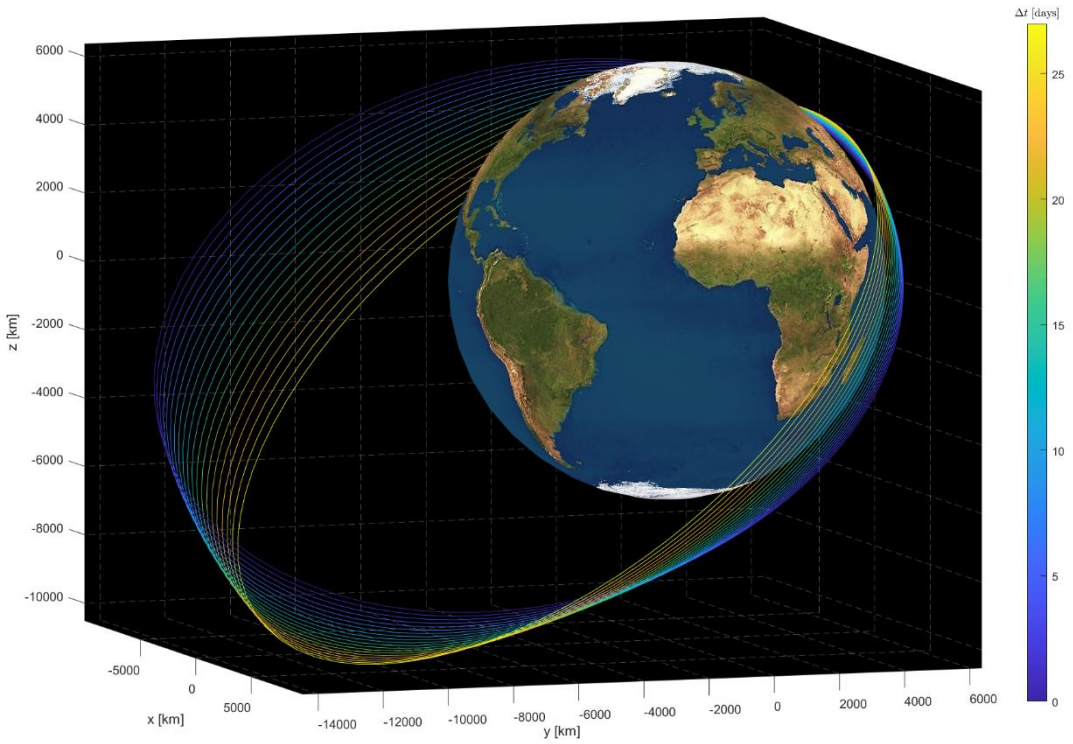

Figure 14 Evolution of orbit size and orientation through 200 orbits

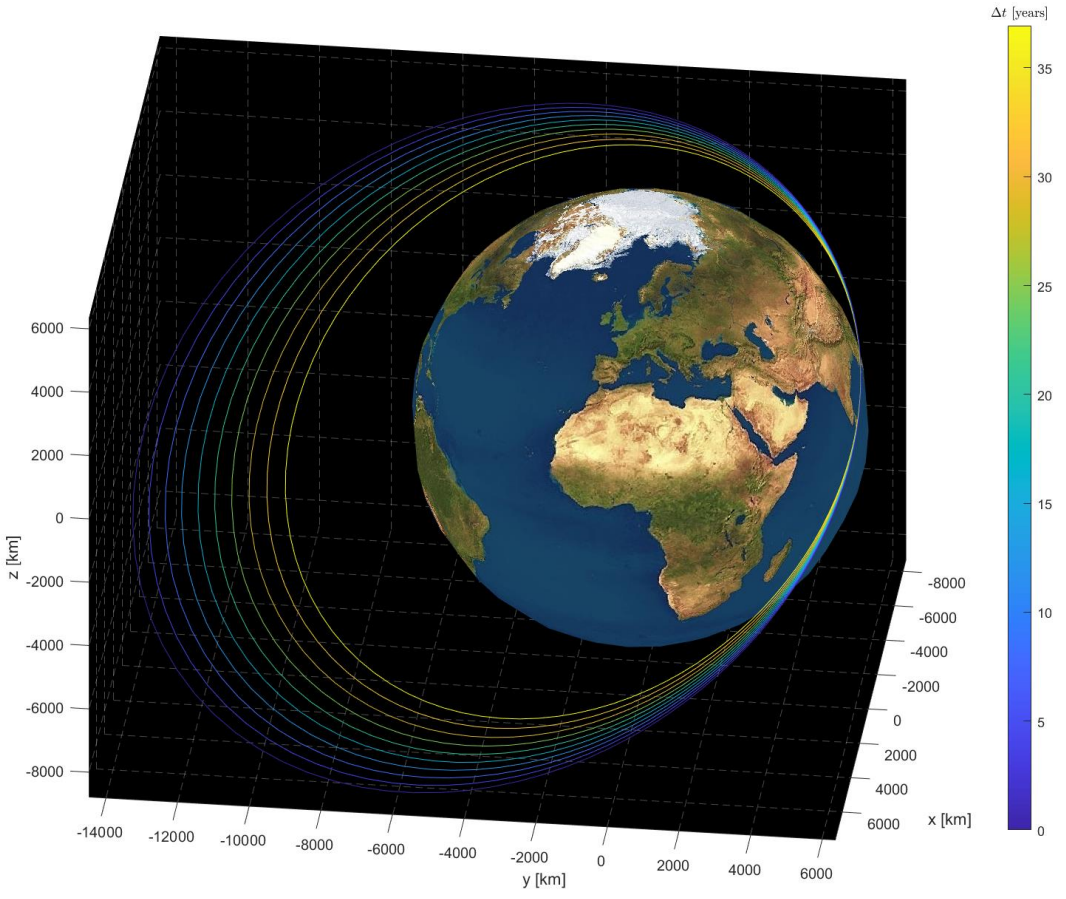

Figure 15 Evolution of orbit size and orientation through 100000 orbits, ignoring J2

2.4 Filtering of High Frequencies

As we have already seen, the time evolution of the Keplerian elements change over longer time periods and have oscillations around these variations. Of course, these just make data harder to represent and read, and might lead to misinterpretation for certain parameters, thus representing only the long-term evolution proves very useful.
The approach that was taken is the one of a moving-average filter: after creating a set time window, whose size was defined through a trial-and-error approach, it will be applied continuously to the evolution of each parameter, replacing the values of each time step with a mean value, computed over the window itself.

As evident from the plots of all parameters, the long-time effects due, for example, to drag on the semi-major axis and eccentricity are much more evident for the green (filtered) plots, while for inclination it's viewable that inclination value remains about constant, while an interpretation of the plot before filtering, would read it as growing over time.

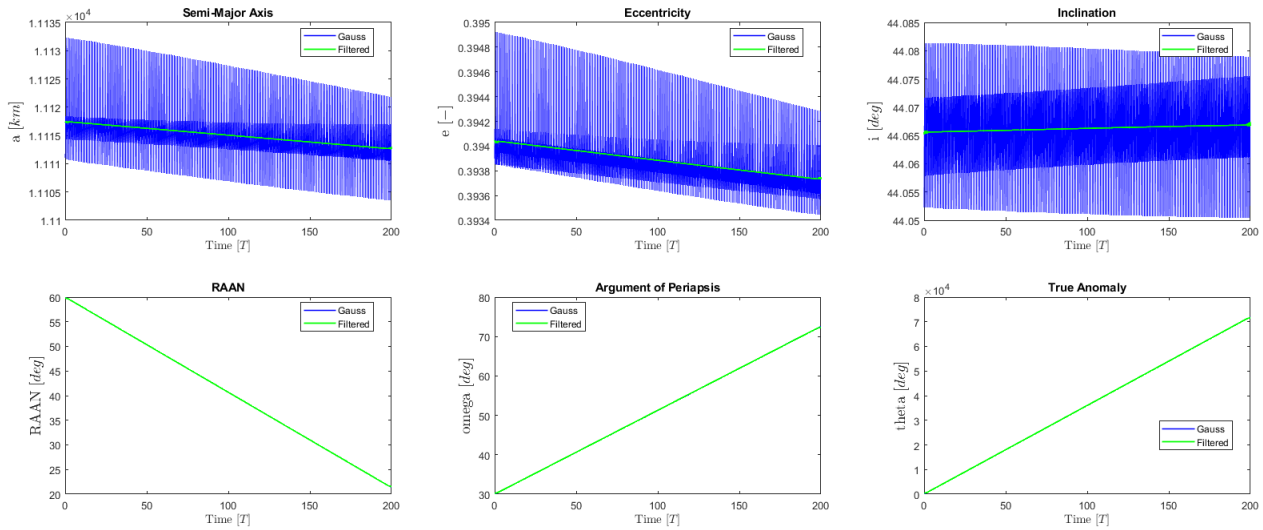

Figure 16 Figure 18 Filtered Keplerian elements obtained through Gauss equations over 200 orbits

2.5 Comparison with Real Data

Gauss equations of this model will be applied to real data of the satellite ARASE (ERG), a JAXA satellite launched on the 20th December 2016 that studies the Van Allen's belts. This spacecraft travels a highly elliptical orbit, with a semi-major axis of about 22721.15 km and an inclination of about 31.665°.
The ephemerides for this spacecraft were generated at https://www.space-track.org as a .txt file, and then read and plotted against results obtained from the model starting from the same initial conditions.
Dimensions and weight of the spacecraft are known, while the drag coefficient will be kept equal to the one of the satellite from the previous analysis, as they are supposed to be similar in shape. A mean cross-section between the smallest and the largest of the satellite will be used, simulating a continuous change of attitude of the satellite in its consecutive near-Earth passages.
The Keplerian elements behaviour will be studied over a 3-year time span, from 1st February 2017 (which is two months after its launch, reason why real data is wiggly for initial time instants) to 1st February 2020.

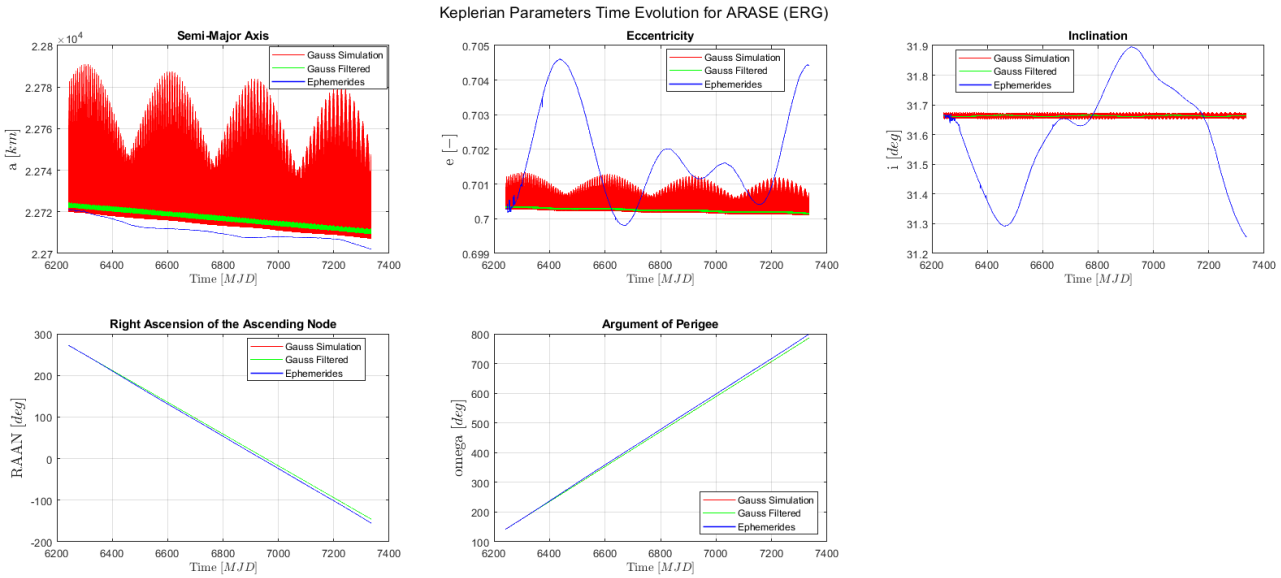

Figure 17 Evolution of Keplerian elements for ARASE (ERG), either ephemerides (Blue) or generated through Gauss equations' simplified model (Red) and filtered (green)

- Semi-major axis from the Ephemerides, which are generated with a time step of about a day, shows a decreasing behaviour over time, similarly to the one obtained from the simplified model, especially after the filter are applied.
- Both Eccentricity and Inclination depend on initial value and don't show the same amplitude of oscillations of real data. Mean value is still close to real data.
- RAAN and Argument of Periapsis show a similar behaviour to real data, with slightly different change rates. This difference, however, is still small even after a 3-years span. This happens because second zonal harmonic is the most influential perturbation on these parameters.

Bibliography

- H. Curtis, Orbital Mechanics for Engineering Students, Second Edition (Aerospace Engineering). 2ndEdition, Butterworth-Heinemann, 2009, ISBN-13 978-0123747785.
- Slides of the course.
- NASA/JPL's HORIZONS web-interface: https://ssd.jpl.nasa.gov/horizons.cgi
- Space-Track: https://www.space-track.org